METHODS 19, 194–212 (1999)
Article ID meth.1999.0851, available online at http://www.idealibrary.com on IDEAL®

Characterization of Heterologous Protein–Protein Interactions Using Analytical Ultracentrifugation

German Rivas,* Walter Stafford,† and Allen P. Minton‡,[1]

*Centro de Investigaciones Biológicas, CSIC, Madrid 28006, Spain; †Boston Biomedical Research Institute, Boston, Massachusetts 02114; and ‡National Institute of Diabetes, Digestive, and Kidney Diseases, National Institutes of Health, Building 8, Room 226, Bethesda, Maryland 20892–0830

Methods for quantitative characterization of heterologous protein–protein interactions by means of analytical ultracentrifugation (AUC) include sedimentation equilibrium, tracer sedimentation equilibrium, sedimentation velocity, and analytical band sedimentation. Fundamental principles governing the behavior of macromolecules in a centrifugal field are summarized, and the application of these principles to the interpretation of data obtained from each type of experiment is reviewed. Instrumentation and software for the acquisition and analysis of data obtained from different types of AUC experiments are described. © 1999 Academic Press

Although the basic principles underlying analytical ultracentrifugation (AUC) were established almost 75 years ago (1), this method still provides one of the most powerful tools for the physicochemical characterization of biological macromolecules and of the interactions between them. There are several reasons for the longevity and vitality of AUC: the essential simplicity of the underlying theory, providing a firm foundation for the interpretation of experimental data; the broad variety of problems accessible to investigation via AUC; a tradition of regularly occurring significant advances in technique and analysis; and, most recently, the commercial availability of modern, state-of-the-art instrumentation. The purpose of this paper is to provide a brief description for the nonspecialist of some of the more "user-friendly" applications of AUC to the detection and quantitative characterization of protein complexes in solution.[2]

Studies of complex formation in solution may have a variety of objectives: the simple detection of complexes and measurement of their abundance under a given set of conditions, characterization of the stoichiometry and structure of complexes, and characterization of reversible association–dissociation equilibria and kinetics. Although AUC is a poor source of information about reaction kinetics, it is one of the most powerful methods for obtaining answers to all of the remaining questions.

In this paper we discuss the application of AUC to the investigation of complexes formed in a solution of two macromolecular components designated A and B, which may combine to form one or more species A_iB_j. A variable associated with a particular species will be subscripted with a pair of stoichiometric indices; for example, the molar mass, molar concentration, and weight/volume concentration of the species A_2B are denoted by M_{21}, c_{21}, and w_{21} respectively.[3] In contrast, a variable subscripted with a single index refers to any single species without reference to the composition of that species.

I. INSTRUMENTATION, ANCILLARY EQUIPMENT, AND SOFTWARE FOR DATA ANALYSIS

There are two distinctly different but complementary instrumental approaches to the acquisition of AUC data, which we have termed "real-time acquisi-

[1] To whom correspondence should be addressed. Fax: (301) 402–0240. E-mail: minton@helix.nih.gov.

[2] Earlier reviews of the use of AUC to study heteroassociations include (2–6).

[3] The possible formation of multiple conformational isomers of complexes with a single stoichiometry is neglected here, although these may in principle be distinguished by differences in their hydrodynamic properties. Extension of the analyses presented here to take these into account is straightforward.

1046-2023/99 $30.00

tion" and "postcentrifugation acquisition." Each of these approaches offers certain advantages (7), and the choice of approach to be used for a particular study should be dictated by the nature of the system being investigated and the conditions under which the study is to be carried out.

The traditional real-time approach involves the use of an analytical ultracentrifuge, that is, an ultracentrifuge equipped with an optical system permitting the measurement of one or more optical signals as a function of radial position while the sample solution is spinning in the centrifuge rotor. While a variety of instruments of this type have been used, to the best of our knowledge the only instruments now manufactured commercially are the XL-A and XL-I analytical ultracentrifuges manufactured by Beckman–Coulter (Fullerton, CA), which are equipped respectively with optics for measurement of gradients of UV and visible absorbance and gradients of absorbance and refractive index. A complete selection of ancillary equipment, including rotors and sample cells, is available from Beckman–Coulter.

The postcentrifugation approach uses a preparative rather than analytical ultracentrifuge, together with ancillary instruments, such as an optical scanner or fractionation device, that permit the measurement of one or more signals as a function of position in the centrifuge tube following the conclusion of the centrifuge run. Various means are employed to ensure the stability of the gradients formed during centrifugation, so that the result of the subsequent measurement is an accurate representation of the gradient(s) existing prior to the termination of the centrifuge run. The earliest measurements of this type were performed to characterize the migration of bands in rate-zonal density gradient centrifugation in large centrifuge tubes (8), but have since been refined to permit accurate acquisition of conventional equilibrium gradients (9–12) and even preequilibrium gradients at a single time point (13, 14). Any of a broad variety of preparative ultracentrifuges commonly encountered in the biomedical research laboratory may be used, subject only to the requirement for accurate speed and temperature control. At present, the only commercially available instrument providing centrifuge tube fractionation with resolution sufficient for satisfactory analysis of equilibrium gradients is the FR-115, manufactured by Brandel (Gaithersburg, MD). The FR-115 may be used with various sizes of cylindrical centrifuge tube ranging in sample volume from <100 μl to several milliliters. Polypropylene adaptors enabling each of these tube types to be centrifuged in conventional swinging-bucket rotors are available from Brandel.

Analysis of data from AUC experiments may be carried out with the assistance of free software available through the Interest Group for Reversible Associations in Structural and Molecular Biology (RASMB), through its site on the World Wide Web (www.bbri.org/rasmb/rasmb.html) and the associated FTP server.[4] Applications described in this review are listed in Table 1. Alternately, the user may elect to analyze data using commercially available nonlinear least-squares modeling software, together with models described in the literature (see below). A package of data analysis software is provided by Beckman–Coulter to purchasers of its analytical ultracentrifuges, but at present, application of this software to analysis of heteroassociating systems is limited.

II. BASIC PRINCIPLES[5]

The flux, or rate of transport, of solute species i in a sector-shaped centrifuge cell spinning at angular velocity ω is described by the relation (1, 18)

$$J_i = s_i w_i \omega^2 r - D_i \frac{dw_i}{dr}, \qquad [1]$$

where J_i is the flux (in the outward direction) of species i in units of mass/area/time, w_i is the weight/volume concentration of species i, ω is the angular velocity of the rotor in radians per second, r is the radial position, and s_i and D_i are respectively the sedimentation and diffusion coefficients of species i. These two quantities are properties of the solute molecule in a particular solvent. The sedimentation coefficient is given by

$$s_i = \frac{M_i(1 - \bar{\nu}_i \rho_0)}{N_A f_{\mathrm{sed},i}}, \qquad [2]$$

where M_i, $\bar{\nu}_i$, and $f_{\mathrm{sed},i}$ denote respectively the molar mass, partial specific volume, and frictional coefficient for sedimentation of species i, ρ_0 denotes the density of solvent, and N_A denotes Avogadro's number. The product $M_i(1 - \bar{\nu}_i \rho_0)$ is referred to as the buoyant mass and is denoted subsequently by M_i^*.[6] The diffusion coefficient is given by

[4] RASMB also hosts a very active on-line discussion group (rasmb@bbri.org) where AUC topics are frequently raised, and requests for assistance and advice are ordinarily responded to quickly and enthusiastically. One may subscribe by writing to the list manager at rasmb-manager@bbri.org.

[5] We restrict this brief introduction to consideration of solutions containing one or more solute species that are so dilute that nonspecific repulsive interactions between solute molecules is insignificant (i.e., the solution is thermodynamically ideal); extensive development of theory, including nonideal behavior, may be found elsewhere (2, 15–17).

[6] The buoyant mass reflects the difference between the mass of the sedimenting solute molecule and the mass of the solvent it displaces. If the particle is less dense than the solvent, its buoyant mass will be negative, and it will sediment inward (i.e., float) rather than outward.

$$D_i = \frac{RT}{N_A f_{\mathrm{diff},i}}, \qquad [3]$$

where R denotes the molar gas constant, T the absolute temperature, and $f_{\mathrm{diff},i}$ the frictional coefficient for diffusion. The two frictional coefficients are functions of the size and shape of the macromolecule as well as its interaction with solvent and other solute molecules. In the ideal limit, these two coefficients are equal (19), so Eqs. [2] and [3] may be combined to yield the Svedberg equation (1)

$$\frac{s_i}{D_i} = \frac{M_i^*}{RT}. \qquad [4]$$

The process of sedimentation of an initially uniform solution at high angular velocity in a sector-shaped centrifuge cell, calculated according to Eq. [1], is illustrated by the series of gradients plotted in Fig. 1A; parameters of the simulation are given in the figure legend. The most rapid and noticeable changes occur at the top (meniscus) and bottom (base) of the solution, where solute is being respectively depleted and pelleted. The region over which solute concentration rises from zero (or from a nonzero meniscus concentration) to the plateau is generally referred to as the boundary. The relatively flat region between the depleted boundary and the accumulated solute at the bottom is called the plateau; solute concentration in this region, initially equal to the loading concentration, slowly decreases with time due to the dilution caused by the increasing cross section with radial distance of the sector-shaped centrifuge cell.

By means of a special boundary-forming sample cell for the analytical ultracentrifuge (20) or a boundary-forming apparatus for cylindrical centrifuge tubes (14), it is possible to layer a small amount of one solution on top of another solution at the outset of a centrifuge run, forming a narrow band of added solution adjacent to the meniscus. If the density of the band is less than that of the solution below it, then macrosolute species in the band—provided that they are sufficiently dilute—will sediment in accordance with Eq. [1].[7] The process of sedimentation of a band of ideal macrosolute, calculated using Eq. [1] with parameters equal to those used to calculate Fig. 1A except for rotor speed, is plotted in Fig. 1B.

As sedimentation proceeds, the radial distribution of each species sedimenting and diffusing in a centrifugal field will tend toward a limit in which the net transport of that species vanishes, i.e., $J_i = 0$ for all i. As a consequence, no further changes in concentration gradients are observed, and the solution is said to be at sedimentation equilibrium.[8] By setting the left-hand

[7] If the density of the solution in the band is greater than that of the solution below it, the band will be unstable in a centrifugal field and rapidly dissipate via convection.

[8] The time required to reach equilibrium is a function of the sedimentation and diffusion coefficients of solutes, the rotor speed, and the length of the solution column. Formulas for estimating the time to equilibrium are given in (21–23).

TABLE 1

Software for Analysis of AUC Data Obtained from Solutions of Two Interacting Macrosolute Components[a]

Name of application [(Author) Operating System]	Brief description: system treated, functionality
SEDEQ [(A. P. Minton) DOS]	Sedimentation equilibrium (SE) of solution containing up to three independently sedimenting species of arbitrary buoyant molar mass. Suite contains MULTISIM for simulation, SEDEQ42 for nonlinear least-squares (nlsq) modeling of absorbance data.
TWOCOMP [(A. P. Minton) DOS]	SE of solution containing two sedimenting components that may reversibly self- and/or heteroassociate to form multiple complexes. Suite contains 2COMPSIM for simulation, 2C1SFIT for nlsq modeling to 1 signal data, 2C2SFIT for modeling to 2 signal absorbance data.
DCDT [(W. F. Stafford) MAC, DOS]	Sedimentation velocity (SV) of solution containing one or more sedimenting species. Corrects for time-invariant baseline artifacts, calculates $g(s^*)$ and signal-average sedimentation coefficient for absorbance, interferometric data.
MULTIFIT [(L. Holladay) WIN]	SV of solution containing up to three independently sedimenting species. Fits absorbance data by approximate solutions to Lamm equation.
SVEDBERG [(J. Philo) WIN]	Same as above, but with different approximate solutions, different user interface.
SEDFIT [(P. Schuck) WIN]	SV of solution containing up to three independently sedimenting species. Corrects for time- and radius-invariant baseline artifacts; fits absorbance, interferometric data by exact numerical solutions to Lamm equation.
ABCDFITTER [(W. F. Stafford) DOS]	SV of solution containing two sedimenting components capable of forming equilibrium heterodimers and trimers. Corrects for time-invariant baseline artifacts; fits absorbance, interferometric data by exact numerical solutions to Lamm equation for two heteroassociating components in rapid equilibrium

[a] Available on the RASMB FTP server as of February 1999.

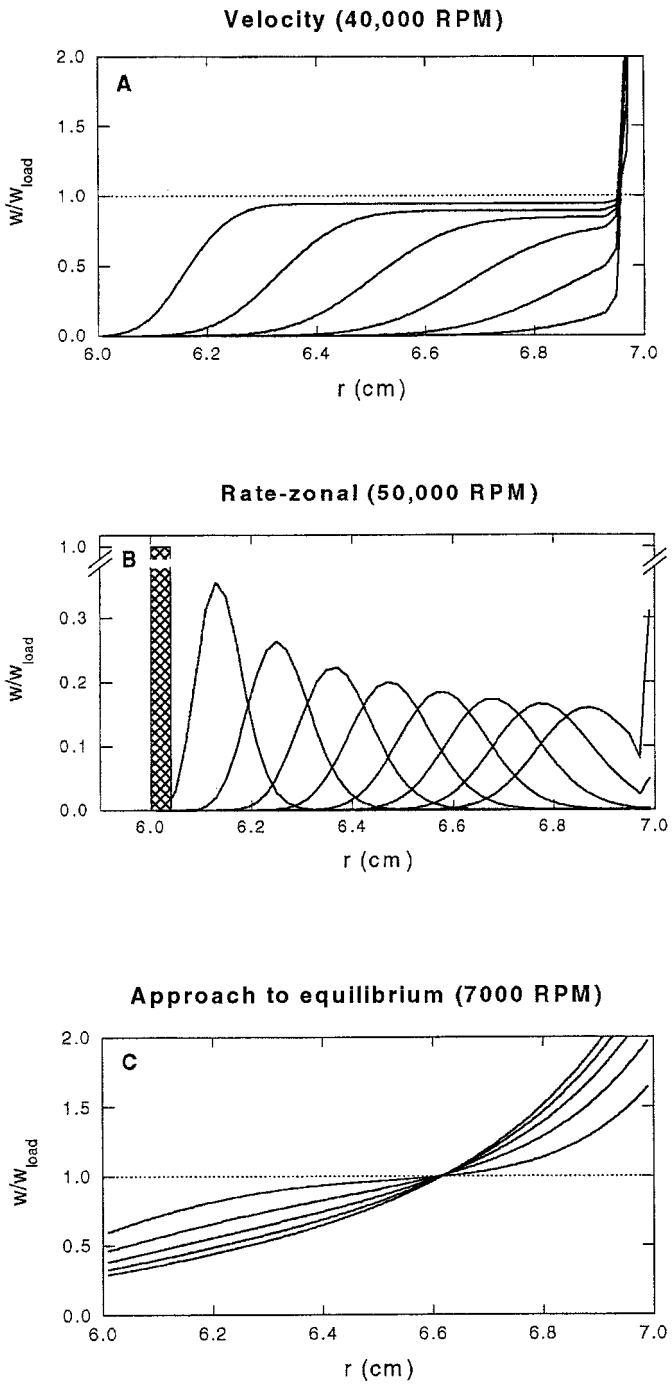

FIG. 1. Simulation of the sedimentation of bovine serum albumin, calculated for a single species with $s = 4.3 \times 10^{13}$ s and $D = 5.9 \times 10^{7}$ cm^2/s via numerical solution of Eq. [1], with $T = 20°C$. w/w_{load} is the ratio of the weight concentration of solute at a given radial position and time to the original (uniform) concentration of solute prior to initiation of centrifugation. (A) Velocity (high-speed) run. Successive gradients correspond to elapsed time intervals of 1 h. (B) Band sedimentation. Cross-hatched area represents layer of macrosolute introduced at time 0. Successive gradients correspond to elapsed time intervals of 0.5 h. (C) Approach-to-equilibrium (low-speed) run. Successive gradients correspond to elapsed time intervals of 16 h, and the final gradient represents a close approximation to sedimentation equilibrium.

side of Eq. [1] to zero and combining the result with Eq. [4], one obtains

$$\frac{d \ln w_i}{dr^2} = \frac{M_i^* \omega^2}{2RT}, \qquad [5]$$

which may be integrated with respect to r^2 to obtain an expression for the equilibrium gradient of an ideally sedimenting solute,

$$w_i(r) = w_i(r_0)\exp\left[\frac{M_i^* \omega^2}{2RT}(r^2 - r_0^2)\right], \qquad [6]$$

where r_0 denotes an arbitrarily selected reference position. The gradient at equilibrium differs fundamentally from any gradient measured prior to attainment of equilibrium in that (1) it is independent of the initial gradient; (2) it is independent of the shape of the centrifuge cell; and (3) it is independent of the hydrodynamic properties of the solute molecule, depending only on the buoyant mass. A simulated approach to equilibrium at low angular velocity, calculated using Eq. [1] starting with an initially uniform solution, is illustrated in Fig. 1C. Parameters are the same as Fig. 1A except for rotor velocity. In this example, the duration of centrifugation required to reach equilibrium was almost 100 h, but equilibrium experiments may be shortened considerably by reducing the length of the solution column, as the time required to reach equilibrium at a constant rotor speed varies roughly as the square of the length of the column (21).

AUC studies are accordingly divided into two basic types: measurement and analysis of the time development of signal gradients at high angular velocity, referred to generically as sedimentation velocity experiments, and measurement and analysis of equilibrium signal gradients obtained at lower angular velocity, referred to generically as sedimentation equilibrium experiments. A third class of experiments, band sedimentation, is a variant of the velocity method, and is described separately. All three types of experiments can provide useful information about the presence and abundance of protein complexes in solution.

The analysis of AUC data obtained from solutions containing two solute components is somewhat more complex than that obtained from solutions of a single solute component, because the individual components may contribute differently to any specific signal being measured. In the present work we restrict ourselves to consideration of signals that are linearly dependent on the weight/volume concentration of each underlying component,

$$S_k(r) = \alpha_{k,A} w_{A,tot}(r) + \alpha_{k,B} w_{B,tot}(r) = \sum_{i,j} \alpha_{k,ij} w_{ij}(r), \qquad [7]$$

where S_k denotes the kth class of signal (corrected for background), $\alpha_{k,x}$ is the constant of proportionality between signal k and weight/volume concentration of pure component X, and $\alpha_{k,ij} \equiv \alpha_{k,A} f_{A,ij} + \alpha_{k,B} f_{B,ij}$, where $f_{x,ij}$ is the mass fraction of component X in A_iB_j.[9] While this condition is satisfied for many types of signals and macrosolutes, it is of course incumbent on the investigator to ascertain that it is true (to within experimental precision) for the particular signal and set of experimental conditions chosen, by means of signal measurements performed on solutions of known composition.

Background and Baseline Signals

All of the analyses to be described in subsequent sections are predicated on the availability of data in the form of signals that are linear in the w/v or molar concentration of solute species and components as indicated in Eq. [7]. Ordinarily, actual experimental data include extra signal contributions from sources other than sedimenting solutes. It is necessary to understand and take account of these extra signals, or eliminate them insofar as possible, to properly analyze that part of the signal that reflects solute behavior.

Radius- and time-independent contributions to the overall observed signal may arise from the presence of one or more unsedimenting (usually small-molecule) solutes in the solution being studied. If these are present in the buffer, the contribution can usually be eliminated by measurement and subtraction of buffer signal. However, if the extra signal is due to contamination of the test solute species, buffer subtraction will not suffice. One common method of correcting for such contamination is to overspeed at the conclusion of a low-speed equilibrium run, after the equilibrium signal gradient(s) has been acquired. The solution is then sedimented at maximum rotor velocity until all macrosolutes are cleared from the innermost region of solution. This is evidenced by the appearance of a radially independent baseline adjacent to the meniscus, the mean amplitude of which may then be measured and subtracted from all points in the equilibrium gradient previously obtained. This method is not applicable when the baseline is subject to significant changes with time.

Radius- and time-independent offsets may also be due to artifacts or limitations of the optical systems used to acquire the signal. For example, interferometric optics permit one to measure differences between the refractive index at different radial positions in the cell, but do not provide an absolute measure of refractive index (and hence concentration) at any point. Hence in a low-speed sedimentation equilibrium experiment carried out with refractometric optics, one must allow for the presence of a constant concentration offset of undetermined magnitude that must be evaluated via model fitting to the data. It should be evident that the necessity of doing so increases the number of variable fitting parameters by one for each radially scanned sample, with consequent reduction in the precision of best-fit parameter values determined by the modeling process (24).

Other types of instrumental artifacts can lead to offsets that vary considerably with radial position (see, e.g., Fig. 7A) and possibly with time as well. Two automated methods for the elimination and/or evaluation of instrumental artifacts in data acquired from the Beckman–Coulter analytical ultracentrifuge have recently been implemented in software programs that are now available through RASMB. The time-derivative method of Stafford (25) is applicable to the analysis of sedimentation velocity data, while the linear least-squares approach of Schuck (26) may be applied to the analysis of both velocity and approach-to-equilibrium data.

Association Equilibria

Analytical ultracentrifugation may be used to detect and characterize macromolecular complexes in solution, independent of whether or not these complexes are in chemical equilibrium with uncomplexed reactants. The presence (or absence) of reversible—as opposed to irreversible—heteroassociations is revealed by the ability (or inability) to quantitatively model one's experimental results in the context of a hypothetical equilibrium association scheme. In such a scheme one postulates the presence of a finite set of heterocomplexes A_iB_j of specified composition, denoted here by $\{ij\}$, together with a corresponding basis set of equilibrium association constants. Depending on circumstances it may be particularly convenient to express species concentrations in terms of one or another set of concentration units that are proportional to each other and to the number density of molecules of that species. These are the weight/volume concentration w_{ij}, the molar concentration $c_{ij} = w_{ij}/M_{ij}$, and the species signal magnitude $S_{k,ij} = \alpha_{k,ij} w_{ij}$, where the signal proportionality constants $\alpha_{k,ij}$ are defined in the text following Eq. [7]. Accordingly, the equilibrium association constant for formation of species $\{ij\}$ from monomeric A and monomeric B may be defined with respect to each of these concentration scales; their definitions and the constants of proportionality between them are given here:

[9] Examples of different classes of signals might be the UV or visible absorbance at different wavelengths, the refractive index, or the activity of a radiolabel. For these respective signals $\alpha_{k,x}$ would represent a specific extinction coefficient, specific refractive increment, or specific radioactivity of component X.

$$K_{ij}^{w} \equiv \frac{w_{ij}}{w_{10}^{i} w_{01}^{j}}, \qquad [8a]$$

$$K_{ij}^{c} \equiv \frac{c_{ij}}{c_{10}^{i} c_{01}^{j}} = \frac{M_{10}^{i} M_{01}^{j}}{M_{ij}} K_{ij}^{w} \qquad [8b]$$

$$K_{ij}^{(k)} \equiv \frac{S_{k,ij}}{S_{k,10}^{i} S_{k,01}^{j}} = \frac{\alpha_{k,ij}}{\alpha_{k,10}^{i} \alpha_{k,01}^{j}} K_{ij}^{w} \qquad [8c]$$

Note that $K_{ij}^{(k)}$ is not defined if either A or B does not contribute to the kth signal.

Given a set of association constants K_{ij}, or equivalent constants that may be defined as functions of the K_{ij} (see below), one may calculate the equilibrium concentrations of all species as a function of the composition of the solution, as specified by the total concentrations of A and B. The general procedure for doing so is illustrated in the Appendix for the example reaction scheme introduced below.

To estimate equilibrium constants from experimental data reflecting signal average properties of the solution, it is essential that conditions be established under which all relevant species can be significantly populated. Consider, for example, the stepwise model (Scheme 1) elaborated in the Appendix. K_{I} can be evaluated with precision only under conditions such that A, B, and AB are all present in significant concentration, and K_{II} can be evaluated with precision only under conditions such that B, AB, and AB_2 are all present in significant concentration. Depending on the relative magnitudes of K_{I} and K_{II}, it may not be possible to measure both constants at a single solution composition. The most efficient way to explore the various possibilities is by means of numerical simulation, as described for the above reaction scheme in the Appendix [see also (27)]. It is imperative to employ global fitting to a series of runs using a range of ratios of total A to total B because of the ambiguities inherent in a two-step binding process. Neither the weight-average molecular weight nor the weight-average sedimentation coefficient will be a single-valued function of the mixing ratio of total A to total B (6). However, a correct (physically possible) solution to the least-squares problem will return calculated values of the loading concentrations of total A and B that are either approximately equal to or less than the known loading concentrations (depending on whether or not mass is conserved or lost during the experiment), while an unphysical solution will return a calculated value of at least one of the two loading concentrations that is significantly greater than the known value.

$$\mathrm{A} + \mathrm{B} \rightleftharpoons \mathrm{AB} \qquad K_{\mathrm{I}}^{w} \equiv K_{11}^{w} = w_{11}/(w_{10}w_{01})$$

$$\mathrm{AB} + \mathrm{B} \rightleftharpoons \mathrm{AB_2} \qquad K_{\mathrm{II}}^{w} \equiv K_{12}^{w}/K_{11}^{w} = w_{12}/(w_{11}w_{01})$$

SCHEME 1

III. SEDIMENTATION EQUILIBRIUM

Consider a solution containing monomeric A (denoted by {10}), monomeric B {01}, and possibly one or more heterocomplexes $\{ij\}$. At sedimentation equilibrium the concentration gradient of signal k is obtained by combining Eqs. [6] and [7],

$$S_k(r) = \sum_{i,j} S_{k,ij}(r) = \sum_{i,j} S_{k,ij}(r_0) \exp\left[\frac{M_{ij}^{*}\omega^2}{2RT}(r^2 - r_0^2)\right], \qquad [9]$$

where $S_{k,ij}(r_0) = \alpha_{k,ij} w_{ij}(r_0)$. Note that Eq. [9] is true, independent of whether or not the heterocomplexes are in equilibrium with each other and with monomeric A and B. The quantities M_{10}^{*} and M_{01}^{*} may be measured independently, by performing sedimentation equilibrium experiments on solutions of the individual components. Providing that the association of A and B is independent of pressure over the range of pressures encountered in the experiment, as is almost always the case for equilibrium experiments conducted at relatively low rotor speed and short column length (28, 29), it follows that

$$M_{ij}^{*} = iM_{10}^{*} + jM_{01}^{*}. \qquad [10]$$

Thus the value of M_{ij}^{*} may be independently calculated for any postulated species in a model, leaving only the corresponding value of $S_{k,ij}(r_0)$ to be determined by curve fitting.[10] Thus the presence of heterocomplexes at significant concentration in a solution mixture of A and B would be evidenced by the failure of the equilibrium gradient to be modeled (to within experimental precision) by an equation of the form of Eq. [9] containing just two terms,

$$S_k(r) = S_{k,10}(r) + S_{k,01}(r), \qquad [11]$$

with two unknown variables to be evaluated via nonlinear least-squares analysis, $S_{k,10}(r_0)$ and $S_{k,01}(r_0)$.[11]

[10] If $\alpha_{k,\mathrm{A}}$ and $\alpha_{k,\mathrm{B}}$ are both ≥ 0, as is ordinarily the case, then $S_{k,ij}(r_0) \geq 0$ for all i and j. To ensure that least-squares modeling does not lead to unphysical values of $S_{k,ij}(r_0)$, it is common practice to employ $\log S_{k,ij}(r_0)$ rather than $S_{k,ij}(r_0)$ as the actual parameter values to be obtained by curve fitting. Since the transformation is obvious, we shall continue to refer to $S_{k,ij}(r_0)$ as the fitting parameters for the sake of didactic clarity.

[11] It is assumed here that for the kth signal, both $\alpha_{k,10}$ and $\alpha_{k,01}$ are nonzero. If, for example, $\alpha_{k,01} = 0$, as would be the case if the kth signal arose from a label that is only attached to component A, then the $S_{k,01}(r)$ term in Eqs. [8] and [10] (and comparable equations to follow) vanishes because monomeric B is "invisible" to a probe of the kth signal. This property is exploited in the technique of tracer sedimentation equilibrium, described below.

If Eq. [11] fails to describe the data to within the precision of measurement, then one explores progressively more complex models until the simplest model accommodating the data is found. The simplest model for heteroassociation would involve the presence of a single heterocomplex $\{ij\}$ of unknown stoichiometry,

$$S_k(r) = S_{k,10}(r) + S_{k,01}(r) + S_{k,ij}(r), \qquad [12]$$

with three unknown parameters $S_{k,10}(r_0)$, $S_{k,01}(r_0)$, and $S_{k,ij}(r_0)$. A variety of possible complex stoichiometries may be tried in a systematic fashion (e.g., $\{11\} \rightarrow \{21\} \rightarrow \{12\} \rightarrow \cdots$) until a satisfactory fit is obtained. It may prove difficult to fit the data to within experimental precision with a model containing only a single complex. In that event, a model containing several complexes, expressed generally as

$$S_k(r) = S_{k,10}(r) + S_{k,01}(r) + \sum_{i,j} S_{k,ij}(r), \qquad [13]$$

may be fit to the data,[12] and by inspection of the relative magnitudes of the best-fit values of the various $S_{k,ij}(r_0)$, it may be possible to determine whether one or more species included in the model are negligible. If so, these species may be eliminated, the simplified model refitted to the data, and the values of the nonnegligible $S_{k,ij}(r_0)$ determined with greater precision.

The following is an example of an analysis carried out according to the procedure described above. In a study of the interaction between α-chymotrypsin (CT) and soybean trypsin inhibitor (STI), Quast and Steffen (30) first centrifuged each protein separately to sedimentation equilibrium to determine the buoyant molar mass of each, and to establish that neither protein self-associated under the conditions of the experiment. Next, a mixture of the two proteins was centrifuged to sedimentation equilibrium and the absorbance gradient plotted in Fig. 2 was obtained. Also plotted in Fig. 2 are the gradients calculated from the best fits of Eq. [10] (no heteroassociation), Eq. [11] (a single complex STI · CT), and Eq. [12] (two complexes STI · CT and STI · CT_2). Analysis of the magnitude and distribution of residuals obtained from the best fits of the respective models indicates that the inclusion of the ternary complex provides a statistically significantly improved fit to the data.[13]

[12] Any particular model should be limited to a small set of complexes (two or three at most), as the ability to fix parameter values with any certainty declines sharply as the number of postulated species increases.

[13] While it is theoretically possible to obtain a fit of equal quality by postulating the presence of the alternate ternary complex $STI_2 \cdot CT$ instead of STI · CT_2, the best-fit values of $S_{290,ij}$ so obtained are grossly incompatible with the known loading concentrations and extinction coefficients of the two proteins at 290 nm, leading to rejection of this model.

It is reiterated here that the above analysis yields no information about whether any detectable complex A_iB_j is in reversible equilibrium with monomeric A and B. To test the hypothesis of reversible equilibrium, one must postulate the existence of a set of one or more association equilibria, specified by the equilibrium constants K^w_{ij} defined in Eq. [8]. If the association of A and B is independent of pressure over the range of pressure encountered in the experiment (as assumed above) then K^w_{ij} is independent of radial position, and it is readily shown (31) that sedimentation equilibrium and chemical equilibrium may be simultaneously achieved at all points in the centrifuged solution. It follows that a general model for $S_k(r)$ may be written as

$$S_k(r) = \alpha_{k,10} w_{10}(r) + \alpha_{k,01} w_{01}(r) + \sum_{i,j} \alpha_{k,ij} K^w_{ij} w^i_{10} w^j_{01}. \qquad [14]$$

Since all of the $\alpha_{k,ij}$ are known functions of the independently determined values of $\alpha_{k,A}$ and $\alpha_{k,B}$, the only parameter values to be determined by fitting are $w_{10}(r_0)$, $w_{01}(r_0)$, and one $K_{w,ij}$ for each complex postulated in any particular model. The reader may have already observed that for a given set of postulated complexes, Eq. [14] contains the same number of undetermined parameters as Eq. [13]; it follows that any

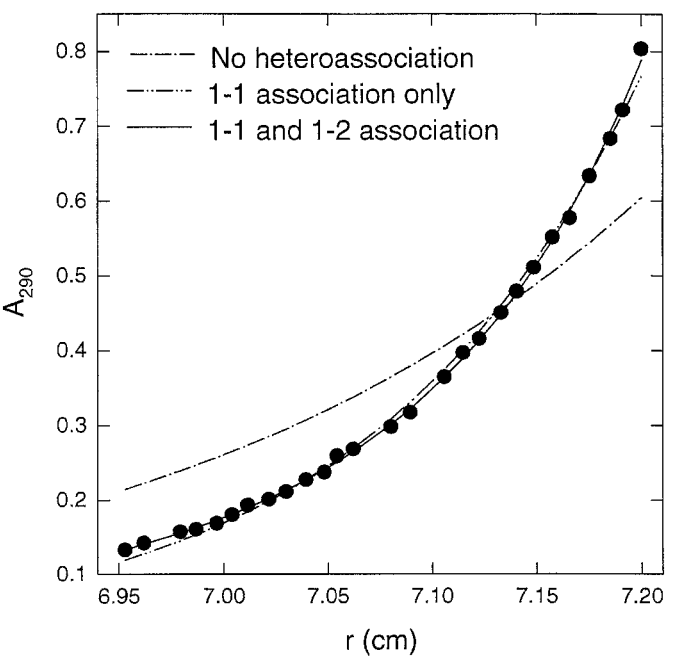

FIG. 2. Equilibrium absorbance gradient of a solution of soybean trypsin inhibitor (w_{load} = 0.062 g/liter) and chymotrypsin (w_{load} = 0.21 g/liter) at 22.5°C and 14,000 rpm. Points: data of Quast and Steffen (30). Curves: dot–dash, best fit of Eq. [10] (no association model); dot–dot–dash, best fit of Eq. [11] (1:1 association model); solid, best fit of Eq. [12], with 1:1 and 1:2 complexes.

single data set[14] that can be modeled to within experimental precision by one of these equations can be modeled by the other. To establish the presence of reversible associations, it is necessary to globally model several data sets obtained from several solutions of different composition (ratio of total A to total B) with the condition that only the values of $w_{10}(r_0)$ and $w_{01}(r_0)$ be allowed to vary between data sets, while the $K_{w,ij}$ are constrained to be the same for all data sets. While global modeling of n_d data sets with a general mixture model specifying n_c complexes (Eq. [13]) would entail determination of the value of $n_d(2 + n_c)$ unknown parameters, modeling the same amount of data with a model specifying n_c equilibrium complexes (Eq. [14]) would entail the determination of only $2n_d + n_c$ unknown parameters. Since this is $n_c(n_d - 1)$ fewer parameters than required by the general mixture model, the ability of Eq. [14] to successfully fit the combined data would thus provide significant evidence for the presence of the proposed equilibria. The software package TWOCOMP (Table 1) fits multiple equilibrium absorbance scans from the XL-A by a model for self- and heteroassociation that allows for the presence of any or all of the complexes {20}, {02}, {11}, {21}, {12}, and {22} in chemical equilibrium with {10} and {01}.

Depending on the system being studied and the instrumentation used, the number of freely variable fitting parameters may be reduced even further by the application of constraints derived from conditions of mass or signal conservation (6, 32–34), by acquiring two or more radially dependent signals (such as absorbance at different wavelengths) that discriminate between the two solute components (34–38), and/or by acquiring data from each sample at multiple rotor speeds (39). The reader is referred to the original publications for descriptions of the various methods for reducing the number of freely variable parameters.

In the absence of even qualitative information obtained from other types of experiments, it is not uncommon or surprising to find that an initial set of sedimentation equilibrium experiments on a particular system yields data that may indicate the presence of significant heteroassociation, yet fail to discriminate between alternate models of heteroassociation and/or fail to yield unambiguous quantitative estimates of postulated equilibrium constants. Hsu and Minton (29) have described a strategy for efficiently designing additional experiments to obtain the most information per experiment. According to this strategy, one uses simulations, constrained to fit the behavior exhibited by the initial set of experiments, to find the solution composition or compositions (loading concentrations of the individual components) at which measured signals are most sensitive to alterations in model parameters and vice versa. Hsu and Minton demonstrated that equilibrium signal gradients obtained at those particular solution compositions contain the most information that can be effectively used to resolve ambiguities in the initial experimental results and, thus, facilitate further characterization of the underlying association equilibria. Simulations of this type were used by Rivas *et al.* (40) to determine solution compositions at which sedimentation equilibrium experiments aimed at quantitative characterization of the heteroassociation between complement subcomponents C1r and C1s could be most efficiently carried out. Optimization of information content in sedimentation equilibrium studies of heteroassociation has also been discussed by Roark (39) and Philo (6).

[14] A data set consists of a measurement of signal as a function of radial distance obtained in a single solution at a single rotor speed.

IV. TRACER SEDIMENTATION EQUILIBRIUM

The use of tracers substantially extends the range of solute concentrations and solution compositions over which sedimentation equilibrium may be characterized experimentally, as the tracer signal is optimized for the particular method of measurement, independent of the total solute concentrations. This provides a very useful way to discriminate between alternative proposed mechanisms of macromolecular association.

A tracer (A*) is generated by labeling one macromolecular species (i.e., A) with a reporter group that provides a signal unique to the labeled component. The experimenter must of course establish that A* is a bonafide tracer, i.e., that the behavior of molecules of A* is physicochemically indistinguishable from that of the corresponding unlabeled molecules of A under the conditions of the experiment. Not only is it necessary that the molar mass of any attached label be less than about 1% of that of the parent macrosolute, but the label must neither facilitate nor inhibit interactions between the tracer and other molecules.

A typical utilization of tracer sedimentation equilibrium to detect and characterize the association between two macromolecular solutes (A and B) would be the following: a series of solutions is prepared containing a fixed small amount of tracer A* sufficient to give the appropriate signal level, together with different amounts of unlabeled B. Each of these solutions is centrifuged to sedimentation equilibrium and the gradient of tracer signal measured by one of the methods described in Section I. Additionally, a gradient of a second signal that is linear in the concentration of B may be measured; this second gradient will reflect the concentration gradient of B independently of that of A, as A* will constitute a negligible fraction of total solute. Any effect of unlabeled B on the signal gradient of A* will reflect heterointeractions between molecules of

A and B (40).[15] In principle, these interactions may be either attractive, leading to the formation of one or more heterocomplexes of A and B, or repulsive, leading to nonideal behavior. This review is limited to consideration of heteroassociations in ideally sedimenting solutions; the characterization of repulsive interactions via sedimentation equilibrium is discussed elsewhere (16, 17, 42).[16]

Experimental systems studied via tracer sedimentation equilibrium fall into two qualitatively distinct categories. In the first category, the reactants are of comparable buoyant mass and heterocomplexes are at most only a few times more massive than the reactants. Under conditions appropriate for the analysis of sedimentation equilibrium, any species present in significant concentration at the base of the solution is present in significant concentration throughout the solution. In the second category, one reactant and/or the heterocomplex(es) are much more massive—by at least an order of magnitude—than the smaller reactant. In such solutions it is possible to clear the heavier species from the region of solution closest to the meniscus, while retaining in this region the lighter free tracer species. Distinct and qualitatively different analyses have been developed to treat each of these categories, which are summarized here in turn.

Category 1: Smaller Range of Sizes of Sedimentable Species

The solutions are centrifuged to equilibrium in short solution columns (no more than 3–4 mm from meniscus to base) at a rotor speed such that the tracer signal at the base is estimated to exceed that at the meniscus by a factor of no more than 3 or 4. Under such conditions, the gradient of tracer signal k should be reasonably well described by the relation

$$S_k(r) = S_k(r_0)\exp\left[\frac{\langle M^*_{w,A}\rangle\omega^2}{2RT}(r^2 - r_0^2)\right]. \qquad [15]$$

The value of the cell-average quantity $\langle M^*_{w,A}\rangle$ may be shown to closely approximate the value of the weight-average buoyant molar mass of A, defined by

$$M^*_{w,A} \equiv \frac{\Sigma_{i,j}\, f_{A,ij} w_{ij} M^*_{ij}}{w_{A,tot}}, \qquad [16]$$

that is characteristic of the loading composition of the solution (40). Each sample scanned thus provides an experimentally measured value of the dependent variable $M^*_{w,A}$ for the particular solution composition specified by the loading concentrations of the two components $\{w_{A,tot}(\text{load}),\ w_{B,tot}(\text{load})\}$. When a sufficient number of measurements have been made over a sufficient range of loading compositions, the experimentally measured dependence of $M^*_{w,A}$ on $w_{A,tot}$ and $w_{B,tot}$ may be modeled by hypothetical reaction schemes to determine the most appropriate reaction scheme and the best-fit values of equilibrium constants in such schemes.

An example of such an analysis may be found in a study of the interactions between complement subcomponents C1r and C1s (40). A summary of the experimental results is shown in Fig. 3. From knowledge of the molar masses of individual peptide chains it is evident, even prior to modeling, that in the absence of C1s, C1r is present as a dimer, and that in the presence of saturating concentrations of C1s, C1r sediments as a $(C1r)_2(C1s)_2$ heterotetramer. Such information provides an important guide to the selection of the most probable association scheme(s). Other studies carried out using this technique, and variations thereof, include characterizations of the heteroassociation of apolipoproteins A-2 and C-1 (35) and the effect of DNA on the association of lambda CI repressor (44).

Category 2: Larger Range of Sizes of Sedimentable Species

To carry out this analysis one must measure individual gradients of both A* and B, i.e., $w_{A,tot}(r)$ and $w_{B,tot}(r)$. If all A_iB_j complexes and free B are depleted from the region ($r < r'$), then all A* present in this

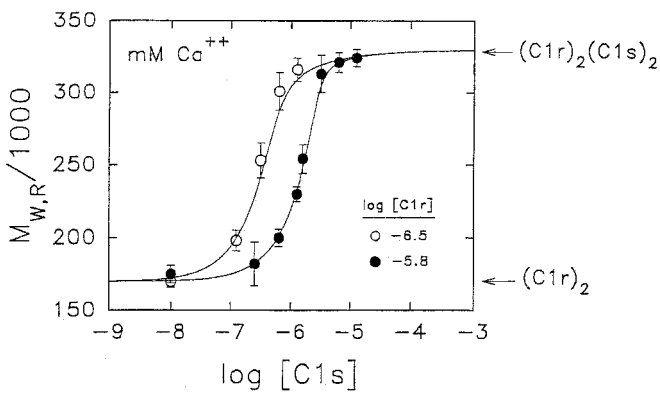

FIG. 3. Effect of unlabeled C1s on the weight-average molar mass of tritium-labeled C1r ($M_{w,R}$) in the presence of 1 mM Ca^{2+}. Different symbols represent results obtained at different concentrations of C1r, as shown in the legend. Asymptotic values of $M_{w,R}$ correspond respectively to the homodimer of C1r subunits and the heterotetramer $(C1r)_2(C1s)_2$. Plotted curves represent the best fit of the following reaction scheme: $(C1r)_2 + C1s \rightleftharpoons (C1r)_2(C1s)$; $(C1r)_2(C1s) + C1s \rightleftharpoons (C1r)_2(C1s)_2$. Adapted from Rivas *et al.* (40).

[15] Note that the identical methodology may be used for detection of self-association as well as heteroassociation, if B is simply unlabeled A (41).

[16] Neglect of repulsive interactions limits the validity of the analysis described here to solutions containing no more than a total of 1–5 mg/ml macromolecular solute under favorable conditions (moderate ionic strength and pH) and much lower concentrations under unfavorable conditions (low ionic strength, low or high pH) (15, 16, 43).

region is free, i.e., $w_{A,free}(r) = w_{A,tot}(r)$ for $r < r'$. An example of such behavior is shown in Fig. 4, taken from a study of the interaction of fibrinogen with platelet fibrinogen receptors (45). Assuming that the solution is at sedimentation equilibrium, the gradient of free A* may be extrapolated to any value of r using Eq. [6] together with the known buoyant molar mass of A* and the value of $w_{A,free}(r_0)$ obtained at the meniscus (or any other $r < r'$). Since the total concentration of A*, $w_{A,tot}(r)$, is known in the region containing complexes, the concentration of bound A* at any value of $r > r'$ may then be calculated as a function of position via simple subtraction:

$$w_{A,bound}(r) = w_{A,tot}(r) - w_{A,free}(r). \qquad [17]$$

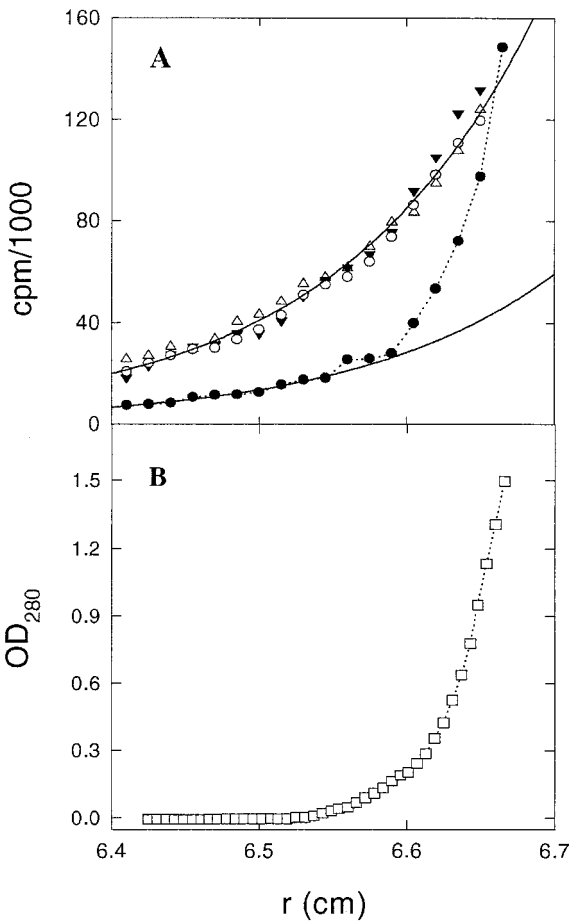

FIG. 4. (A) Gradient of ^{125}I-labeled fibrinogen (Fbg*) in the absence and presence of integrin αIIbβ3. Loading concentration of tracer is equal for all data sets. Triangles, open circles: gradients of label [proportional to $w_{Fbg,tot}(r)$] in the absence of binding to integrin; closed circles: gradient of label in the presence of integrin under binding conditions; curves: calculated gradients of unbound Fbg* [proportional to $w_{Fbg,free}(r)$]. (B) Gradient of unlabeled integrin in the same centrifuge tube. Reproduced from *J. Mol. Recog.*, G. Rivas, K. Tangemann, A. P. Minton, and J. Engel, Copyright John Wiley & Sons Limited. Reproduced with permission.

One can then tabulate the value of $w_{A,bound}(r)/w_{B,tot}(r)$ as a function of $w_{A,free}(r)$ for all data acquired in the region $r > r'$, and analyze this model-independent result—equivalent to a binding isotherm—in the context of postulated schemes for equilibrium binding of A to B. The data presented in Fig. 4 were analyzed to yield the dependence of fibrinogen binding on free fibrinogen concentration plotted in Fig. 5. Other applications of this method and variations thereof include characterization of the binding of glycolytic enzymes to fibrous actin (46) and the binding of platelet glycoprotein IIb peptide 656–657 to fibrinogen (47).

Labeling Techniques

It cannot be too strongly stressed that successful utilization of the tracer sedimentation equilibrium methods described above depends crucially on the use of a label that provides the necessary sensitivity and linearity, while not perturbing the interactions to be explored. Traditional protein labeling reactions tend to produce heterogeneous products (e.g., labeling at multiple histidine and/or lysine residues), whereas recombinant technology enhances the ability of the investigator to insert a label at a unique site on a protein (48, 49). When a chromophoric or fluorophoric label (50) is used, it is essential to determine whether the signal for a fixed concentration of tracer varies with the concentration of unlabeled species present. If so, corrections for composition-dependent response must be developed and applied [for an example of such a correction, see (43)].

Postcentrifugation acquisition of tracer gradients provides the investigator with several additional options, including the ability to use radiolabeled tracers. Although many nonradioactive methods of labeling have been developed (50, 51), in our opinion radiolabeling (52, 53) still remains the "gold standard" of labeling techniques for quantitative purposes, due to the small size of the label,[17] the strong signal available from isotopes with relatively short half-lives, and the demonstrated linearity of signal. The measurement of radiolabel activity in fractions of small volume has been remarkably simplified by the use of Beckman–Coulter Ready Caps, containing a solid scintillant, in place of scintillation fluid (12).

A vastly broader scope of investigation is provided by the ability to perform a tracer sedimentation equilibrium experiment on a solution containing an unlabeled (and hence unperturbed) tracer protein. Subsequent to establishment of sedimentation equilibrium and fractionation, the tracer component is labeled, and its concentration gradient measured via a chemically or im-

[17] The size difference between tracer and unlabeled parent, as well as the extent of chemical perturbation, may be reduced to almost zero via metabolic labeling (48, 49).

munochemically specific reaction (e.g., an ELISA assay) carried out on samples taken from each of a series of radial fractions (53a).

V. SEDIMENTATION VELOCITY

Sedimentation velocity analysis of interacting systems can provide a wealth of information complementary to that obtained from sedimentation equilibrium analysis. There are at least four general approaches to the analysis of heterologous interacting systems by sedimentation velocity.

1. Using the Centrifuge to Measure Concentrations of Free and Bound Species at Equilibrium

If both A and the complex sediment significantly faster than the "ligand" B, then after a certain period of centrifugation at high speed, the region of the solution closest to the meniscus will be fully depleted of A and any B associated with it. Thus the centrifuge can be used to measure the concentration of free ligand and, by subtraction from the known total (loading) concentration of B, the concentration of bound B, for various loading concentrations of A and B, enabling a binding isotherm to be constructed. This method was used by Revzin and von Hippel (54) to measure the equilibrium association constant for binding of *Escherichia coli lac* repressor to nonoperator DNA. Another example of the use of this method is the measurement of the equilibrium association constant for binding of skeletal heavy meromyosin and myosin subfragment to F-actin (55). In the above studies, absorption optics were used to measure the concentration of unbound protein. The ratio of free ligand to (total minus free) ligand was measured at a series of total concentrations to determine the binding isotherm. This method is a direct measurement of equilibrium concentrations and requires no measurements of sedimentation coefficients.

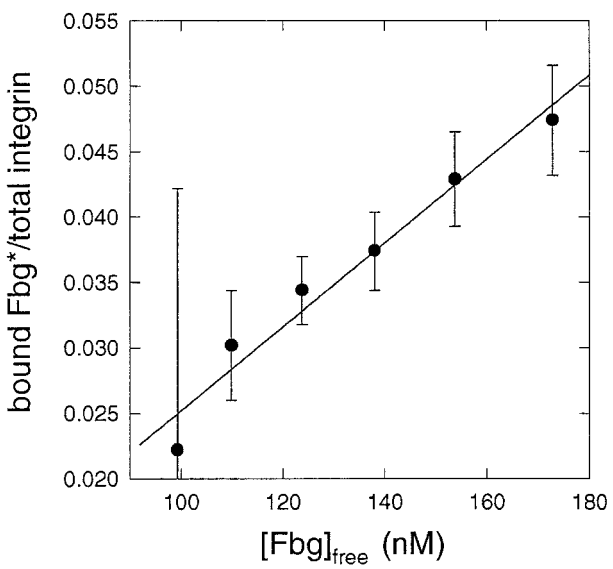

FIG. 5. Plot of calculated ratio $y \equiv [\text{Fbg}]_{\text{bound}}/[\text{integrin}]_{\text{total}}$ as a function of $[\text{Fbg}]_{\text{free}}$. The plotted line represents the best fit of the equation $y = nK_{\text{A}}[\text{Fbg}]_{\text{free}}$. The slope of this line is interpreted as nK_{A}, the product of number of Fbg binding sites per integrin molecule and the equilibrium association constant for individual site binding. Reproduced from *J. Mol. Recog.*, G. Rivas, K. Tangemann, A. P. Minton, and J. Engel, Copyright John Wiley & Sons Limited. Reproduced with permission.

2. Measuring and Modeling the Signal Average Sedimentation Coefficient as a Function of Loading Concentrations

The signal-average sedimentation coefficient is obtained from a background-corrected data set by simple integration over the boundary of absorbance or refractive index. The integration must start at the meniscus if the meniscus concentration is finite (and known) or in a region of zero concentration and zero gradient just centrifugal to the meniscus and end at a radial position where the concentration gradient is zero (i.e., the integration must start and stop where there is no contribution to transport from diffusion).[18] Integration yields the following signal-average squared position of the boundary,

$$\langle r^2\rangle^{(k)} \equiv \frac{\int_{S_{k,\text{men}}}^{S_{k,\text{plat}}} r(S_k)^2 dS_k}{S_{k,\text{plat}} - S_{k,\text{men}}}, \qquad [18]$$

where $r(S_k)$ is the position of the boundary corresponding to a given signal level, $S_{k,\text{men}}$ is the value of the kth signal at the meniscus, and $S_{k,\text{plat}}$ is the value of the kth signal at the plateau. A plot of $\ln(\langle r^2\rangle^{(k)})$ versus $2\omega^2 t$ then has a slope of $\langle s\rangle^{(k)}$, the signal-average sedimentation coefficient, defined as

$$\langle s\rangle^{(k)} = \frac{\sum_{i,j} s_{ij} S_{k,ij}}{\sum_{ij} S_{k,ij}} = \frac{\sum_{i,j} s_{ij}\alpha_{k,ij} w_{ij}}{\sum_{i,j} \alpha_{k,ij} w_{ij}}, \qquad [19]$$

where s_{ij} is the sedimentation coefficient of species $\{ij\}$,[19] and w_{ij} is the concentration of species $\{ij\}$ in the plateau region (2).

When data are acquired with interference optics, it is usual to assume that the $\alpha_{k,ij}$ (in this case, the refractive increments) are equal for all protein species. This

[18] This restriction may prevent measurement of the signal-average sedimentation coefficient if there are a wide range of sedimentation coefficients, as it may be impossible to obtain a sufficient number of radial scans for which there exist both a fully depleted meniscus region and a measurable plateau region.

[19] Sedimentation coefficients will be denoted by a lowercase s to distinguish them from experimental signals, denoted by an uppercase S.

assumption is usually good to within about ±5% (56, 57). Under such conditions $\langle s \rangle^{(k)}$ is approximately equal to the weight-average sedimentation coefficient. However, the assumption may not be quantitatively valid when one of the proteins is heavily glycosylated. When absorbance optics are used, the assumption of species invariant $\alpha_{k,ij}$ is not generally valid for heterologous systems, since the specific extinction coefficients of the two components, $\alpha_{k,A}$ and $\alpha_{k,B}$, may be significantly different at any arbitrarily selected wavelength. However, signal average quantities may be modeled directly, since independently measured or precalculated values of each of the $\alpha_{k,ij}$ can be incorporated into the fitting function.

Equation [19] is valid whether or not the various sedimenting species are in chemical equilibrium. If the various species are in chemical equilibrium, $\langle s \rangle^{(k)}$ may be reformulated as a function of equilibrium constants and the concentrations of monomeric A and B,

$$\langle s \rangle^{(k)} = \frac{\sum_{i,j} s_{ij} \alpha_{k,ij} K_{ij}^{w} w_{10}^{i} w_{01}^{j}}{\sum_{i,j} \alpha_{k,ij} K_{ij}^{w} w_{10}^{i} w_{01}^{j}}, \qquad [20]$$

where w_{10} and w_{01} are, respectively, the concentrations of monomeric A and monomeric B within the plateau region.

Under favorable conditions equilibrium association schemes may be deduced and equilibrium association constants evaluated via nonlinear least-squares modeling of the dependence of the signal-average sedimentation coefficient on solution composition (total concentrations of A and B in the plateau region). However, an analysis of this type requires knowledge of the sedimentation coefficients of individual species, in addition to a model for association equilibria (such as the example provided in the Appendix). The values of s_{10} and s_{01} can usually be measured directly in solutions of the individual components. In the simplest heteroassociating system (i.e., formation of a single 1:1 complex), if the association constant is great enough, the value of s_{11} may be obtained by extrapolation of the measured value of $\langle s \rangle^{(k)}$ to limiting high solute concentration in a solution containing a stoichiometric ratio of the two components. In more complex system, it may be impossible to measure independently the sedimentation coefficient of each complex, and recourse must be made to hydrodynamic models (58) or to curve fitting as described below, in which the sedimentation coefficients of the complexes are treated as variable parameters. If the proteins involved are essentially globular (i.e., axial ratio less than about 1:4) then one can often make use of a rule-of-thumb that s varies as $M^{2/3}$ for a series of geometrically similarly shaped molecules (2).

Since sedimentation coefficients estimated using approximate hydrodynamic theory are intrinsically less reliable than calculated buoyant molar masses, modeling the composition dependence of the signal-average sedimentation coefficient is correspondingly a less reliable method of characterizing solution association equilibria than modeling the composition dependence of signal-average buoyant molar masses obtained from sedimentation equilibrium. However, because of the rapidity of sedimentation velocity measurements relative to ordinary sedimentation equilibrium measurements, this method can in principle be used to obtain information about solution associations of proteins that are too unstable to provide reliable sedimentation equilibrium data. Using the enhancement of sensitivity afforded by signal-averaging techniques such as the time-derivative method described below, sedimentation velocity can be used to conduct experiments at solute concentrations that are significantly lower than those accessible to conventional optical measurements of equilibrium gradients, hence permitting investigation of more strongly interacting systems than otherwise possible in the analytical ultracentrifuge.

3. Analysis of the Time Derivative of the Signal Gradient

A time-derivative method for processing sedimentation velocity data has been developed by Stafford and coworkers (25, 59). The time-derivative method is based on the premise that the systematic background components that are invariant with time are completely eliminated when the time derivative of the signal gradient is computed. The resulting background-free time-derivative data can be averaged and converted to a distribution function, $g_k(s^*)$ versus s^*, where s^* is an apparent sedimentation coefficient defined as

$$s^* \equiv \frac{1}{\omega^2 t} \ln\left(\frac{r}{r_{men}}\right). \qquad [21]$$

The time-derivative method is illustrated in Fig. 6. One starts with a series of signal profiles, each of which is rapidly acquired over a period sufficiently short that diffusion is negligible (Fig. 6A). In the Beckman–Coulter analytical ultracentrifuge, a radial scan of refractive index can be repeated as often as every 8 s, and a scan of absorbance, as often as every minute. The profiles are then subtracted in pairs to produce a series of time difference patterns approximating the time derivative of the signal profile at constant radius (Fig. 6B). The time-derivative curves may be transformed from a function of radius to a function of s^* according to Eq. [21], and then averaged at constant s^* to increase the signal-to-noise ratio (Fig. 6C). The averaged time-derivative curves are then converted to the apparent sedimentation coefficient distribution function $g_k(s^*)$ (Fig. 6D) according to (25, 59)[20]

[20] Equations [22] and [23] have been generalized from those presented in (59) to allow for the possibility of nonuniform $\alpha_{k,ij}$ in multicomponent systems.

$$g_k(s^*) \equiv \left(\frac{\partial S_k}{\partial s^*}\right)_t = \left[\left(\frac{\partial S_k}{\partial t}\right)_r + 2\omega^2 \int_0^{s^*} s' \left(\frac{\partial S_k}{\partial s'}\right)_t ds'\right] \times \left[\left(\frac{\partial t}{\partial s^*}\right)_r\right] \quad [22]$$

The signal-average sedimentation coefficient $\langle s\rangle^{(k)}$ may then be computed from the $g_k(s^*)$ patterns using

$$\langle s\rangle^{(k)} \cong \frac{\int_0^\infty s^* g_k(s^*) ds^*}{\int_0^\infty g_k(s^*) ds^*}. \quad [23]$$

The program DCDT (Table 1) calculates $g_k(s^*)$ from a time series of interferometric or absorbance scans, and then calculates $\langle s\rangle^{(k)}$ from $g_k(s^*)$ as described above. A modified version of DCDT is included in the data analysis package provided by Beckman–Coulter to purchasers of the XL-A or XL-I analytical ultracentrifuge.

Analysis of the composition dependence of $\langle s\rangle^{(k)}$ as measured by this technique proceeds as described in the previous section, via nonlinear least-square modeling using Eq. [19] together with an equilibrium model for the dependence of w_{10} and w_{01} on K_{ij}^w, $w_{\mathrm{A,load}}$, and $w_{\mathrm{B,load}}$.

A great deal of information can be obtained from a simple visual analysis of time-derivative patterns. For example, to identify a two-step binding reaction and distinguish it from a 1:1 complex, one can vary the initial ratios of A and B to differentially populate the singly bound and doubly bound species. In the example shown in Fig. 7, a dimeric single-chained antibody (sFv) and its antigen are mixed in ratios 1:4 and 4:1 to reveal the two bound species, AB and AB_2 (60). If this reaction had been a simple 1:1 complex, only a single complex AB would have formed and only one new boundary would have been seen (Fig. 7c). Figure 7B shows a dilution series of the system shown in Fig. 7A, mixed 1:2. The curves have been normalized to show the shift to dissociated species at the lower concentrations around 50 and 30 nM. By comparison to quantitative simulations of this system (27) we may deduce that value of the dissociation constant K_d ($=1/K_{11}^c$) is less than about 0.1 nM.

Figure 7C shows $g(s^*)$ analysis of an antigen–antibody system that forms a 1:1 complex and demonstrates the utility of $g(s^*)$ analysis to distinguish easily between 1:1 and 2:1 binding stoichiometries; a 1:1 stoichiometry will show only a single peak for the complex for all ratios of A to B. A 2:1 stoichiometry will show two different peaks corresponding to the 1:1 and 2:1 complexes depending on which of the components is in excess as long as the complexes are substantially populated at the concentrations used.

4. Global Fitting to Numerical Solutions of the Lamm Equation: The Todd–Haschemeyer Method

There are useful approximate analytical solutions to the sedimentation-diffusion equations for nonequilibrium mixtures of solute species (61–65), which can be used for detection and quantification of aggregates. The programs MULTIFIT and SVEDBERG (Table 1) fit such models to a time series of velocity scans. However, direct fitting of sedimentation velocity profiles (i.e., solute concentration or signal as a function of radial position and time) with analytical functions is not possible for most interacting systems because even approximate closed form solutions of the underlying sedimentation-diffusion reaction equations do not exist for reversibly associating systems. Therefore, nonlinear curve-fitting procedures, requiring numerical solutions to the sedimentation–diffusion equation, must be used for the analysis of reversibly associating systems. When Eq. [1] is combined with the equation of continuity, one obtains the so-called Lamm equation for a single ideally sedimenting species (2, 18), which relates the time dependence of the concentration of species i at a single position to the radial dependence of that species at a single time:

$$\left(\frac{\partial c_i}{\partial t}\right)_r = -\frac{1}{r}\left[\frac{\partial}{\partial r}\left(s_i\omega^2 r^2 c_i - D_i r \frac{\partial c_i}{\partial r}\right)\right]_t. \quad [24]$$

When the molar concentrations c_i appearing in Eq. [24] are converted to units of weight/volume concentration and thence to signal (via Eq. [7]), and summed over all species, one obtains an expression for the time derivative of the signal at a fixed radial position due to transport (sedimentation and diffusion):

$$\left[\frac{\partial S_k}{\partial t}\right]_r^{\mathrm{xport}} = \frac{1}{r}\frac{\partial}{\partial r}\left[r \sum_{i,j} \alpha_{k,ij}\left(D_{ij}\frac{\partial w_{ij}}{\partial r}\right)_t - \omega^2 r^2 \sum_{i,j} \alpha_{k,ij} s_{ij} w_{ij}\right]. \quad [25a]$$

When the sedimenting species react with each other chemically, the signal at a fixed radial position may also vary with time due to the progress of reaction between species at that position,

$$\left[\frac{\partial S_k}{\partial t}\right]_r^{\mathrm{rxn}} = f(\{w_{ij}\}, \{\alpha_{k,ij}\}, \{\text{rate constants}\}), \quad [25b]$$

where the functional dependence indicated on the right-hand side of Eq. [25b] is dictated by the particular reaction or set of reactions modeled (65a). Thus the

entire dependence of signal on time at a fixed radial position is given by

$$\left[\frac{\partial S_k}{\partial t}\right]_r = \left[\frac{\partial S_k}{\partial t}\right]_r^{\text{xport}} + \left[\frac{\partial S_k}{\partial t}\right]_r^{\text{rxn}}. \qquad [25c]$$

Numerical integration of Eq. [25c] provides the calculated dependence of total signal on both radial position and time, which constitutes the data to be modeled. Nonlinear curve fitting of velocity data thus requires (1) experimental or theoretical values of s_{ij} and D_{ij}, (2) an equilibrium model of the type presented in the Appendix for calculation of (time- and position-dependent) w_{ij},[21] (3) an iterative algorithm for choosing new trial values for independently variable parame-

[21] It is conventionally assumed that all species at a given radial position achieve chemical equilibrium at a rate that is rapid relative to the rate of transport of any species. In this limit the solution to Eq. [25b] depends only on the ratio of forward and backward rate constants (i.e., the equilibrium constant) for a particular elementary reaction step, and not on the values of the individual rate constants (65a).

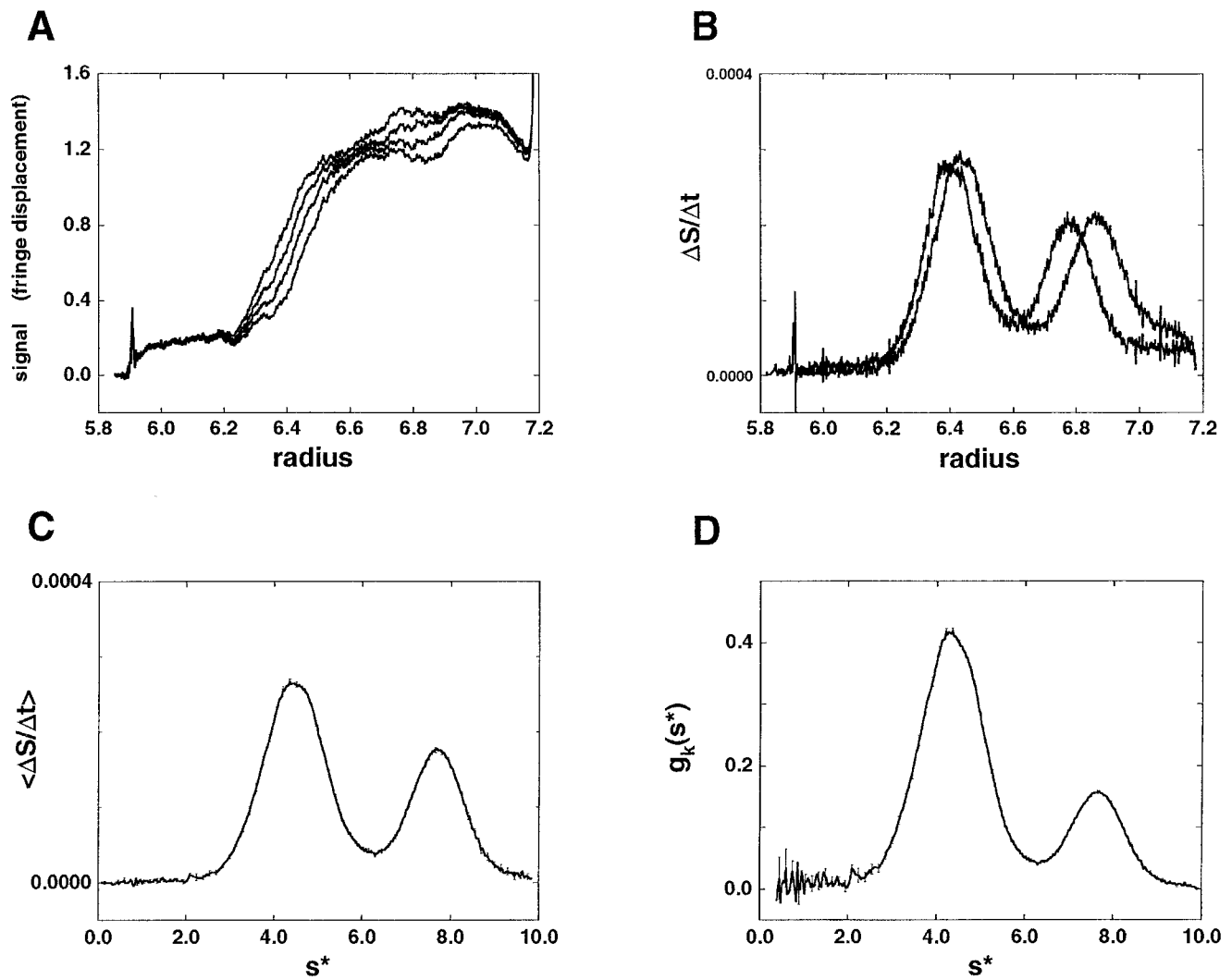

FIG. 6. Time derivative method of sedimentation velocity analysis, exemplified with a solution mixture of a recombinant extracellular domain of a macromolecular antigen c-erbB-2 (ECD) (MW = 90K) and a dimeric single-chain antibody $(sFv')_2$ (MW = 52K). Run at 50,000 rpm at 20°C in an eight-hole titanium rotor. Total concentration of solute is assumed to be proportional to fringe displacement in interferometric optics. (A) Refractive index profiles obtained with the interference optical system of the Beckman–Coulter Optima XL-I analytical ultracentrifuge. Twenty scans were acquired at 90-s intervals over a period of about 30 minutes. (B) Time difference curves, approximating the time derivative, plotted as a function of radius. Curves were obtained by subtracting pairs of refractive index curves 15 min apart at corresponding radial positions. (C) Refined time derivative curves obtained by averaging the curves in (B) after aligning them on the s^* axis (Eq. [22]). Converting radius to s^* takes into account the different times of sedimentation of the original refractive index curves. The time used to compute s^* is the harmonic mean of the times corresponding to the pair being subtracted. (D) Plot of $g_k(s^*)$ versus s^* obtained by transforming dS_k/dt into dS_k/ds^* using Eq. [23] (25, 59).

ters, and (4) a numerical method for solving Eq. [25] given a set of trial parameter values and the independent variables r and t. An error function (usually the weighted sum of the squares of the residuals) is minimized with respect to variation in the trial parameter values until the global minimum is reached. This approach to the analysis of sedimentation velocity data was first published by Todd and Haschemeyer in 1981 (66), who described the use of the finite-element method of Claverie (67) to provide rapid solutions to the Lamm equation for multiple independent species or a single component undergoing a rapid monomer–$n$mer equilibrium, combined with a curve-fitting procedure for evaluating model parameters. Their method has been implemented for nonequilibrium mixtures of ideally sedimenting species in a software program for the analysis of absorbance data obtained on the XL-A (68). An extremely rapid finite-element method for the solution of the Lamm equation has been developed by Schuck *et al.* (69, 70) and implemented in the program SEDFIT (Table 1), which can be used to fit models for multiple independently sedimenting species or a single rapidly self-associating component to a time series of velocity scans obtained on the XL-A or XL-I analytical centrifuge (71).

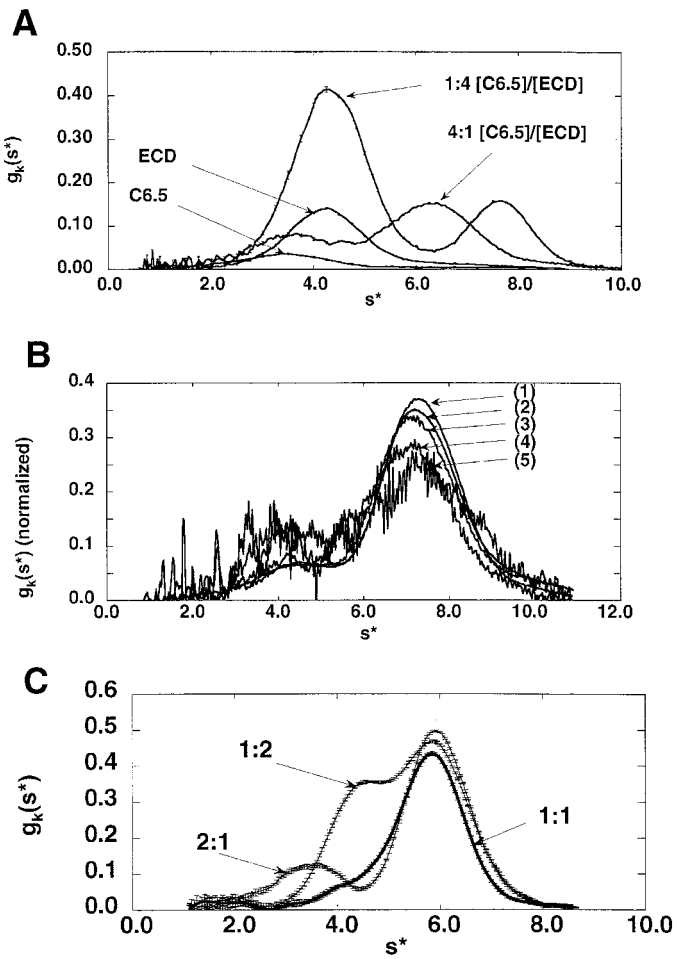

FIG. 7. Qualitative use of $g_k(s^*)$ to demonstrate two-step binding and reversible dissociation at low concentration. (A) ECD and sFv run alone and mixed at 1:4 and 4:1 molar ratios as indicated. (B) Dilution series of the 1:2 mixture. y Axis is normalized $g_k(s^*)$; x axis is s^*. (1) 0.270 mg/ml, 1.16 μM sFv, 2.32 μM ECD; (2) 0.098 mg/ml, 0.42 μM sFv, 0.84 μM ECD; (3) 0.030 mg/ml, 0.13 μM sFv, 0.26 μM ECD; (4) 0.016 mg/ml, 0.07 μM sFv, 0.14 μM ECD; (5) 0.007 mg/ml, 0.03 μM sFv, 0.06 μM ECD. (C) Demonstration of the formation of a 1:1 complex between an Fab and ECD. [Fab]:[ECD] ratios: (1) 1:2, (2) 1:1, (3) 2:1.

The Todd–Haschemeyer method has been adapted by Stafford (72) to the analysis by sedimentation velocity data from heterologous interacting systems obtained with both the absorbance and the interference optical systems. In previous methods, signal-versus-radius data sets have been modeled directly; in this newer approach, signal time difference data are modeled, as illustrated in Fig. 8. Pairs of experimental traces (Fig. 8, top) are subtracted at corresponding radial positions to produce curves of ΔS_k versus radius (Fig. 8, bottom). The use of time difference data completely eliminates any time-independent baseline contributions to the patterns, thereby obviating the need to perform extra optical blank runs to correct the data. This fitting procedure has been implemented in a software program called ABCDFITTER (Table 1). ABCDFITTER is capable of simultaneously fitting the equilibrium association model presented in the Appendix to sedimentation velocity data (multiple scans) obtained from each of several runs carried out at different rotor speeds and using different optical systems. It assumes that the buoyant molar masses, partial specific volumes, and extinction coefficients or refractive index increments of all species are known and further assumes that s_A and s_B are known from separate measurements. It returns as global parameters the values of s_{11}, s_{12}, K_I, and K_{II} in addition to the initial loading values of $w_{A,tot}$ and $W_{B,tot}$ for each run as local parameters.

An example the results of global fitting to delta-S data obtained experimentally (W. F. Stafford, D. Szczesna, T. Tao, and J. D. Potter, unpublished) is shown in Fig. 9. Troponin C (TnC) and troponin I (TnI) were added in 1:1 stoichiometry and run in three cells at different loading concentrations in the presence of EDTA. The independently measured sedimentation coefficients and buoyant molar masses of TnC and TnI were used as fixed input parameters. The initial loading concentrations of each component were input and allowed to float as local parameters since the actual values were not determined separately with sufficient accuracy to allow them to be held constant in the fit. The value of the sedimentation coefficient of the complex and the equilibrium constant were treated as global variables.

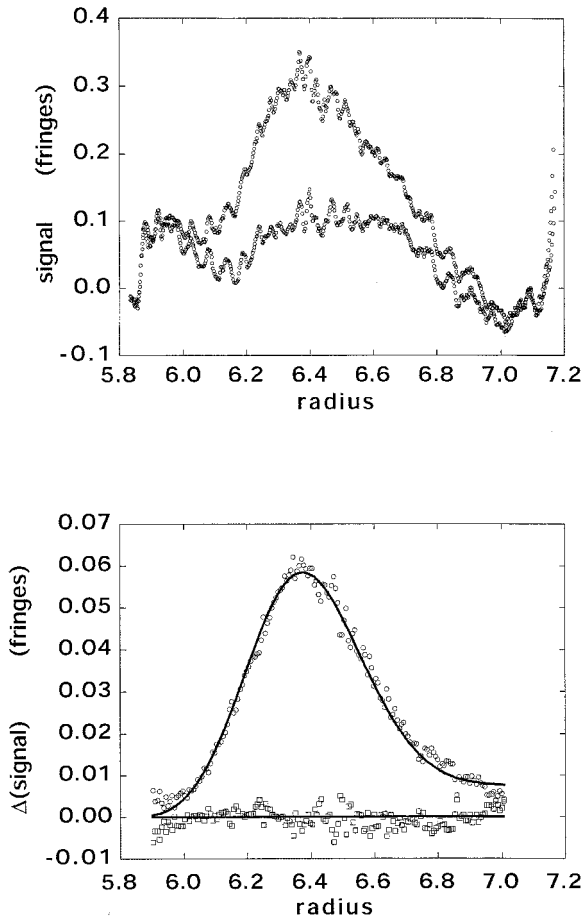

FIG. 8. Nonlinear curve fitting to concentration–time difference, delta-C versus *r*, curves for 1:1 complex formation between troponin C and troponin I in the presence of EDTA. Seventy to eighty concentration profiles, in the form of fringe displacement versus radius, were combined from each of three cells spanning the range of initial loading concentrations as indicated below. The data from all three cells were fit globally to determine K_{11} and S_{11}. *Top:* Two of a total of two hundred ten experimental concentration profiles are plotted as a function of radius. The total loading concentration is 0.120 mg/ml and corresponds to about 0.3 fringe total displacement across the boundary. Note the relatively large systematic background error arising from optical inhomogeneities in the windows and optics. Since these background components are invariant with time, they are removed by subtracting pairs of profiles obtained at different times from the same cell. *Bottom:* (open circles) The difference pattern obtained by subtracting the two curves shown in the top panel; (solid curve) the best fit obtained for this particular curve from the global fit to all 105 difference profiles from the three cells. Each best-fit difference pattern is generated by subtracting the corresponding pairs of curves generated by the procedure of Claverie as described in the text. The run was carried out at 20°C and 56,000 rpm in a Model-E analytical ultracentrifuge equipped with an on-line interferometer system. The nonlinear least-squares fit converged at ±0.0069 fringe RMS and returned $s_{11} = 3.09$S and $K_{11}^c = 1.99 \times 10^5$ M^{-1} as global parameters, and the following values for the initial cell loading concentrations (mg/ml) of TnC and TnI, respectively, as local parameters for each sample: cell 1—0.407, 0.556; cell 2—0.152, 0.155; cell 3—0.049, 0.056 mg/ml. The best-fit value of K_{11}^c agrees quite well with estimates obtained previously by other methods (77), and the returned values of the loading concentrations agree with the known loading concentrations. The residuals are plotted (open circles) below the fitted data. Data close to the meniscus and close to the base, before the so-called hinge point, were not included in the fits.

VI. ANALYTICAL BAND SEDIMENTATION

Early applications of analytical band centrifugation were carried out using preparative (8) and analytical (20) ultracentrifuges. While data obtained at a single time point—the conclusion of a run in the preparative ultracentrifuge—did suffice to allow the evaluation of sedimentation coefficients with useful accuracy and precision, use of the analytical ultracentrifuge provided the capability to obtain gradients at multiple times rather than a single time, with correspondingly improved estimates of both sedimentation and diffusion coefficients. In the early studies, preformed gradients of sucrose or self-forming gradients of salt (e.g., CsCl) at high concentration were used to prevent convection. Since substantial gradients of concentration of low-molecular-weight solutes result in a gradient of both the solvent viscosity and buoyant mass of sedimenting solutes, application of this method required the use of calibrating marker substances to properly evaluate the sedimentation coefficient. It has been recently demonstrated that high concentrations of added cosolvents are not necessary; convection may be prevented by the use of D_2O–H_2O mixtures or physiological buffers such as phosphate-buffered saline (73). Under such conditions, the sedimentation and diffusion coefficients of solute species sedimenting in the band become independent of position (to a very good approximation), and the resulting time dependence of band position and shape may be interpreted on the basis of first principles, i.e., the Lamm equation, rather than by interpolation between calibration standards.

Siegel and Schumaker (74) and Lakatos (75) used analytical band centrifugation in a sucrose gradient to characterize association equilibria between complement subcomponent C1q and activated and inactivated forms of subcomponents C1r and C1s. Under the conditions of the experiment the sedimentation coefficient of uncomplexed C1q is greater than that of the largest complex of C1r and C1s ($C1r_2C1s_2$). Thus a band of ^{125}I-labeled C1q (C1q*) at trace concentration, initially layered on top of a solution of unlabeled reaction partner, sediments through a uniform concentration of reaction partner (equal to the loading concentration), and remains in dynamic chemical equilibrium with it for the duration of the experiment.

Following sedimentation in a cylindrical centrifuge tube in a preparative ultracentrifuge for a fixed period, the tube contents were fractionated according to radial position and the relative amount of tracer in each fraction number *f*, $t(f)$, was determined by gamma counting (bottom of Fig. 9). It was observed that C1q* sedimented more rapidly as the concentrations of unlabeled C1r and/or C1s increased, reflecting a greater equilibrium average degree of complexation. The radial position of the midpoint of the tracer band,

r_t, was determined from the location of half-maximal counts on a plot of cumulative signal $\sum_{f'=1}^{f} t(f')$ versus f (top of Fig. 9). Given the midpoint band positions (r_1 and r_2) of two nonassociating marker solutes of independently known sedimentation coefficients (s_1 and s_2) sedimenting for the same length of time in the same solution under the same conditions, the signal-average sedimentation coefficient of the tracer may be calculated from the interpolation formula[22]

$$\frac{\langle s\rangle^{(k)} - s_1}{s_2 - s_1} = \frac{\ln r_t - \ln r_1}{\ln r_2 - \ln r_1}. \qquad [26]$$

The dependence of $\langle s\rangle^{(k)}$ on the composition of the solution is then analyzed in the context of equilibrium association models, as described in the preceding section.

VII. CONCLUSION

Analytical ultracentrifugation provides a broad variety of techniques for the detection and characterization of protein heterocomplexes in solution. It is essential to keep in mind that AUC is definitely not a "one-size-fits-all" approach. When selecting an experimental technique or a set of techniques to use in the pursuit of the answer to a particular scientific question, one should consider the relative strengths and weaknesses of the various techniques described here with respect to the particular system studied. It may prove to be the case that no individual technique can adequately answer the entire question, and that a combination of techniques is required. Questions such as (but not limited to) the following should be addressed:

How stable are the purified proteins under the desired conditions? (Is the duration of the experiment a consideration?)

Do the individual proteins self-associate? (Must an association model include self- as well as heteroassociation?)

Would the sought heterocomplexes be present in detectable abundance at total solute concentrations that can be quantified by a particular technique? (Does this technique provide sufficient signal?)

Can one of the components be labeled in a particular way without perturbing or inhibiting sought-for heteroassociations?

Are there heterocomplexes in addition to or instead of the simple 1:1 complex? (How broad a range of concentrations is required to fully characterize multiple modes of heteroassociation?)

What level of accuracy and precision in the raw data is required to obtain valid answers to the questions posed? (What is the easiest and simplest way to obtain the necessary accuracy/precision?)

Do the two (unlabeled and/or labeled) components have signals that are sufficiently distinct to enable one to take advantage of the increased resolving power of global analysis of multiple signal gradients?

It is clear that individually or in combination, the techniques described in this minireview should be capable of providing reliable answers to almost any qualitative or quantitative question that may be asked about (steady-state) protein–protein associations in solution. The old dog called analytical ultracentrifugation continues to learn—and perform—new tricks.

[22] The analysis described is strictly valid only for sedimentation in a cylindrical tube (i.e., having constant cross section) when the sedimentation coefficient is independent of position, but is a good approximation in the presence of small density gradients.

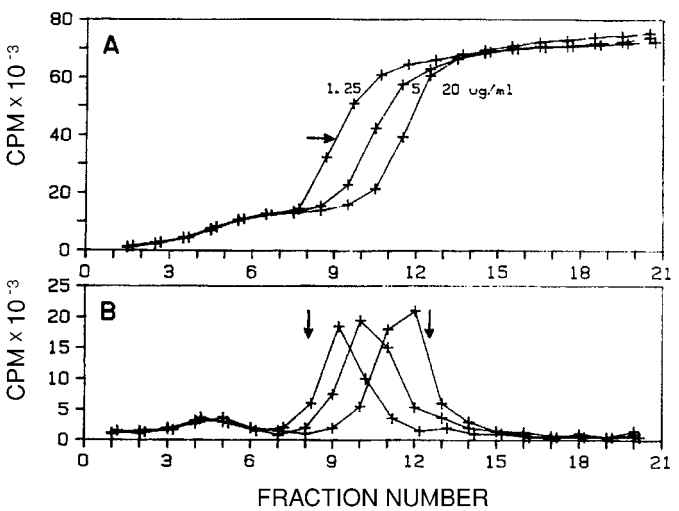

FIG. 9. Analytical band centrifugation of radiolabeled C1q (loading concentration, 2.5 ng/ml) in solutions containing unlabeled $C1r_2C1s_2$ at concentrations of 1.25, 5, and 20 μg/ml (74). Tubes were centrifuged at 59,000 rpm for 4.5 h at 5°C, then fractionated. (B) Counts per fraction plotted against fraction number, which varies linearly with radial distance. Arrows indicate band positions in the absence (left arrow) and presence of $C1r_2C1s_2$ in the limit of high concentration (right arrow). (A) Cumulative counts plotted against fraction number. Arrow indicates half-maximal cumulative signal, corresponding to midpoint of band. Reprinted from *Mol. Immunol.*, **20,** R. C. Siegel and V. N. Schumaker, pp. 53–66, Copyright 1983, with permission from Elsevier Science.

APPENDIX: CALCULATION OF SPECIES ABUNDANCE AND SIGNAL CONTRIBUTIONS FOR A MODEL SET OF HETEROASSOCIATION EQUILIBRIA

Let the formation of AB and AB_2 be described as shown previously in Scheme 1. The calculation of species abundance is facilitated by the conversion of the

equilibrium constants to molar units as shown in Eqs. [8a]–[8c]:

$$K_{\mathrm{I}} \equiv \frac{c_{11}}{c_{10}c_{01}} = K_{\mathrm{I}}^{w}\,\frac{M_{10}M_{01}}{M_{11}}, \qquad [A1]$$

$$K_{\mathrm{II}} \equiv \frac{c_{12}}{c_{11}c_{01}} = K_{\mathrm{II}}^{w}\,\frac{M_{11}M_{01}}{M_{12}}. \qquad [A2]$$

The total molar concentrations of A are given by

$$c_{\mathrm{A,tot}} = c_{10} + c_{11} + c_{12}, \qquad [A3]$$

$$c_{\mathrm{B,tot}} = c_{01} + c_{11} + 2c_{12}. \qquad [A4]$$

Equations [A1]–[A4] may be combined and rearranged to yield the expression

$$b_3 c_{01}^3 + b_2 c_{01}^2 + b_1 c_{01} - c_{\mathrm{B,tot}} = 0, \qquad [A5]$$

where

$$b_3 = K_{\mathrm{II}}K_{\mathrm{I}},$$

$$b_2 = K_{\mathrm{I}} + K_{\mathrm{I}}K_{\mathrm{II}}(2c_{\mathrm{A,tot}} - c_{\mathrm{B,tot}}),$$

$$b_1 = K_{\mathrm{I}}(c_{\mathrm{A,tot}} - c_{\mathrm{B,tot}} + 1).$$

Equation [A5] may be analytically or numerically solved [see, e.g., (76)] to yield c_{01} as a function of K_{I}, K_{II}, $c_{\mathrm{A,tot}}$, and $c_{\mathrm{B,tot}}$. Given the value of c_{01}, the concentrations of all remaining species may be calculated according to

$$c_{10} = c_{\mathrm{A,tot}}/(1 + K_{\mathrm{I}}c_{01} + K_{\mathrm{I}}K_{\mathrm{II}}c_{01}^2), \qquad [A6]$$

$$c_{11} = K_{\mathrm{I}}c_{10}c_{01}, \qquad [A7]$$

$$c_{12} = K_{\mathrm{II}}c_{11}c_{01}. \qquad [A8]$$

Given the molar concentrations c_{ij}, it follows from Eq. [7] and following that the magnitude of the kth signal associated with each species is given by

$$S_{k,ij} = (iM_{\mathrm{A}}\alpha_{k,\mathrm{A}} + jM_{\mathrm{B}}\alpha_{k,\mathrm{B}})c_{ij}. \qquad [A9]$$

ACKNOWLEDGMENTS

The authors thank Dr. P. Schuck, NIH, for critical review of early drafts of this review. A.P.M. dedicates his contribution to the memory of Paul A. Srere, gentleman, scholar, colleague, and friend. His keen insight and wit will be sorely missed.

REFERENCES

1. Svedberg, T., and Pedersen, K. O. (1940) The Ultracentrifuge, Oxford Univ. Press, London; reprinted by Johnson Reprint Corp., New York, 1950.
2. Schachman, H. K. (1959) Ultracentrifugation in Biochemistry, Academic Press, New York.
3. Minton, A. P. (1990) *Anal. Biochem.* **190,** 1–6.
4. Behlke, J., and Ristau, O. (1997) *Eur. Biophys. J.* **25,** 325–332.
5. Minton, A. P. (1997) *Prog. Colloid Polym. Sci.* **107,** 11–19.
6. Philo, J. (1999) *Methods Enzymol.*, in press.
7. Darawshe, S., and Minton, A. P. (1994) *Anal. Biochem.* **220,** 1–4.
8. Martin, R. G., and Ames, B. N. (1961) *J. Biol. Chem.* **236,** 1372–1379.
9. Pollet, R. J. (1985) *Methods Enzymol.* **117,** 3–27.
10. Howlett, G. J. (1987) *Methods Enzymol.* **150,** 447–463.
11. Minton, A. P. (1989) *Anal. Biochem.* **176,** 209–216.
12. Darawshe, S., Rivas, G., and Minton, A. P. (1993) *Anal. Biochem.* **209,** 130–135.
13. Attri, A., and Minton, A. P. (1984) *Anal. Biochem.* **136,** 407–415.
14. Muramatsu, N., and Minton, A. P. (1988) *Anal. Biochem.* **168,** 345–351.
15. Chatelier, R. C., and Minton, A. P. (1987) *Biopolymers* **26,** 507–524.
16. Chatelier, R. C., and Minton, A. P. (1987) *Biopolymers* **26,** 1097–1113.
17. Wills, P., Georgalis, Y., Dijk, J., and Winzor, D. (1995) *Biophys. Chem.* **57,** 37–46.
18. Lamm, O. (1929) *Ark. Math. Astron. Fys.* **21**B(2), 1–4.
19. Tanford, C. (1961) Physical Chemistry of Macromolecules, Wiley, New York.
20. Vinograd, J., Bruner, R., Kent, R., and Weigle, J. (1963) *Proc. Natl. Acad. Sci. USA* **49,** 902–910.
21. Van Holde, K., and Baldwin, R. (1958) *J. Phys. Chem.* **62,** 734–743.
22. Richards, E. G., Teller, D. C., and Schachman, H. K. (1968) *Biochemistry* **7,** 1054–1076.
23. Chatelier, R. C. (1988) *Anal. Biochem.* **175,** 114–119.
24. Brooks, I., Wetzel, R., Chan, W., Lee, G., Watts, D. G., Soneson, K. K., and Hensley, P. (1994) *in* Modern Analytical Ultracentrifugation (Schuster, T. M., and Laue, T. M., Eds.), pp. 15–36, Birkhäuser, Boston.
25. Stafford, W. F. (1992) *Anal. Biochem.* **203,** 295–301.
26. Schuck, P., and Demeler, B. (1999) *Biophys. J.* **76,** 2288–2296.
27. Stafford, W. F. (1994) *in* Modern Analytical Ultracentrifugation (Schuster, T. M., and Laue, T. M., Eds.), pp. 119–137, Birkhäuser, Boston.
28. Kegeles, G., Kaplan, S., and Rhodes, L. (1968) *Ann. N.Y. Acad. Sci.* **164,** 183–191.
29. Hsu, C., and Minton, A. P. (1991) *J. Mol. Recog.* **4,** 93–104.
30. Quast, U., and Steffen, E. (1975) *Hoppe-Seyler's Z. Phys. Chem.* **356,** 617–620.
31. Adams, E. T., Jr. (1968) *Ann. N.Y. Acad. Sci.* **164,** 226–244.
32. Nichol, L. W., and Ogston, A. G. (1965) *J. Phys. Chem.* **69,** 4365–4367.
33. Lewis, M. S. (1991) *Biochemistry* **30,** 11716–11719.
34. Minton, A. P. (1994) *in* Modern Analytical Ultracentrifugation (Schuster, T. M., and Laue, T. M., Eds.), pp. 81–93, Birkhäuser, Boston.

35. Servillo, L., Brewer, H., and Osborne, J. (1981) *Biophys. Chem.* **13,** 29–38.
36. Lewis, M. S., Shrager, R. I., and Kim, S.-J. (1994) *in* Modern Analytical Ultracentrifugation (Schuster, T. M., and Laue, T. M., Eds.), pp. 94–115, Birkhäuser, Boston.
37. Schuck, P. (1994) *Prog. Colloid Polym. Sci.* **94,** 1–13.
38. Bailey, M. F., Davidson, B. E., Minton, A. P., Sawyer, W. H., and Howlett, G. J. (1996) *J. Mol. Biol.*, **263,** 671–684.
38a. Winzor, D. J., Jacobsen, M. P., and Wills, P. R. (1998) *Biochemistry* **37,** 2226–2233.
39. Roark, D. E. (1976) *Biophys. Chem.* **5,** 185–196.
40. Rivas, G., Ingham, K. C., and Minton, A. P. (1994) *Biochemistry* **33,** 2341–2348.
41. Rivas, G., Ingham, K. C., and Minton, A. P. (1992) *Biochemistry* **31,** 11707–11710.
42. Rivas, G., and Minton, A. P. (1999) *Biochemistry* **38,** 9379–9388.
43. Muramatsu, N., and Minton, A. P. (1989) *J. Mol. Recog.* **1,** 166–171.
44. Laue, T., Senear, D., Eaton, S., and Ross, J. (1993) *Biochemistry* **32,** 2469–2472.
45. Rivas, G., Tangemann, K., Minton, A. P., and Engel, J. (1996) *J. Mol. Recog.* **9,** 31–38.
46. Lakatos, S., and Minton, A. P. (1991) *J. Biol. Chem.* **266,** 18707–18713.
47. Calvete, J., Rivas, G., Schäfer, W., and Niewiarowski, S. (1993) *FEBS Lett.*, 335.
48. Ross, J., Senear, D., Waxman, E., Kombo, B., Rusinova, E., Huang, Y., Laws, W., and Hasselbacher, C. (1992) *Proc. Natl. Acad. Sci. USA* **89,** 12023–12027.
49. Cornish, V., and Schultz, P. (1994) *Curr. Opin. Struct. Biol.* **4,** 601–607.
50. Waggoner, A. (1995) *Methods Enzymol.* **246,** 362–373.
51. Cosma, A. (1997) *Anal. Biochem.* **252,** 10–14.
52. Slater, R. (1990) Radioisotopes in Biology: A Practical Approach, IRL Press, Oxford.
53. Kelman, Z., Naktinis, V., and O'Donnell, M. (1995) *Methods Enzymol.* **262,** 430–442.
53a. Liu, J., Reitz, B., Fox, J., and Shire, S. J. (1997) *Pharm. Res.* **14,** 348.
54. Revzin, A., and von Hippel, P. H. (1977) *Biochemistry* **16,** 4769–4776.
55. Margossian, S. S., and Lowey, S. (1978) *Biochemistry* **17,** 5431–5439.
56. Perlman, G. E., and Longsworth, L. G. (1948) *J. Am. Chem. Soc.* **70,** 2719–2724.
57. Babul, J., and Stellwagen, E. (1969) *Anal. Biochem.* **28,** 216–221.
58. Garcia de la Torre, J. (1992) *in* Analytical Ultracentrifugation in Biochemistry and Polymer Science (Harding, S. E., Rowe, A. J., and Horton, J. C., Eds.), pp. 333–345, Roy. Soc. of Chem., Cambridge.
59. Stafford, W. F. (1997) *Curr. Opin. Biotechnol.* **8,** 14–24.
60. Adams, G. P., McCartney, J. E., Tai, M. S., Oppermann, H., Huston, J. S., Stafford, W. F., Bookman, M. A., Fand, I., Houston, L. L., and Weiner, L. M. (1993) *Cancer Res.* **53,** 4026–4034.
61. Holladay, L. (1979) *Biophys. Chem.* **10,** 187–190.
62. Holladay, L. (1980) *Biophys. Chem.* **11,** 303–308.
63. Philo, J. S. (1994) *in* Modern Analytical Ultracentrifugation (Schuster, T. M., and Laue, T. M., Eds.), pp. 156–170, Birkhäuser, Boston.
64. Philo, J. S. (1997) *Biophys. J.* **72,** 435–444.
65. Behlke, J., and Ristau, O. (1997) *Biophys. J.* **72,** 428–434.
65a. Fujita, H. (1975) Foundations of Ultracentrifugal Analysis, Chap. 4, Wiley, New York.
66. Todd, G. P., and Haschemeyer, R. H. (1981) *Proc. Natl. Acad. Sci. USA* **78,** 6739–6743.
67. Claverie, J. M., Dreux, H., and Cohen, R. (1975) *Biopolymers* **14,** 1685–1700.
68. Demeler, B., and Saber, H. (1998) *Biophys. J.* **74,** 444–454.
69. Schuck, P., and Millar, D. B. (1998) *Anal. Biochem.* **259,** 48–53.
70. Schuck, P., MacPhee, C. E., and Howlett, G. J. (1998) *Biophys. J.* **74,** 466–474.
71. Schuck, P. (1998) *Biophys. J.* **75,** 1503–1512.
72. Stafford, W. F. (1998) *Biophys. J.* **74,** A301.
73. Lebowitz, J., Teale, M., and Schuck, P. (1998) *Biochem. Soc. Trans.* **26,** 745–749.
74. Siegel, R. C., and Schumaker, V. N. (1983) *Mol. Immunol.* **20,** 53–66.
75. Lakatos, S. (1987) *Biochem. Biophys. Res. Commun.* **149,** 378–384.
76. Press, W. H., Flannery, B. P., Teukolsky, S. A., and Vetterling, W. T. (1987) Numerical Recipes: The Art of Scientific Computing, Cambridge Univ. Press, Cambridge.
77. Grabarek, Z., and Tao, T. (1992) *J. Muscle Res. Cell Motil.* **13,** 383–393.